JCTC Journal of Chemical Theory and Computation

Article

pubs.acs.org/JCTC

Chelation-Induced Quenching of Two-Photon Absorption of Azacrown Ether Substituted Distyryl Benzene for Metal Ion Sensing

N. Arul Murugan,*[,†] Robert Zaleśny,[†,∥] Jacob Kongsted,[‡] and Hans Ågren[†]

[†]Division of Theoretical Chemistry and Biology, School of Biotechnology, KTH Royal Institute of Technology, SE-10691 Stockholm, Sweden

[∥]Theoretical Chemistry Group, Institute of Physical and Theoretical Chemistry, Wrocław University of Technology, Wyb, Wyspiańskiego 27, PL-50370 Wrocław, Poland

[‡]Department of Physics, Chemistry and Pharmacy, University of Southern Denmark, Campusvej 55, DK-5230 Odense M, Denmark

Supporting Information

ABSTRACT: Imaging of metal ion concentration, distribution, and dynamics can pave the way to diagnose a number of diseases and to identify the normal functioning of the human body. Recently, two-photon microscopy-based imaging of metal ions has become popular due to several favorable factors as compared to fluorescence-based imaging. However, much has to be investigated in order to design probes with large two-photon absorption cross sections and yet with selective binding affinity toward metal ions. In particular, it is crucial to recognize the mechanisms of metal ion-induced changes of the two-photon absorption intensity. The present paper contributes to this effort and reports on the results of extensive studies carried out to define a reliable computational protocol that can account for sampling, solvent, and finite temperature effects for one- and two-photon properties of metal probes, using azacrown ether substituted distyrylbenzene embedded in solvents as a testbed. We employ a selection of theoretical approaches to model the structure of the probe alone and in the presence of Mg^{2+} ion in acetonitrile solvent, including static quantum-chemical calculations, rigid- and flexible-body molecular dynamics, and hybrid QM/MM molecular dynamics. For a set of solute–solvent configurations, the one- and the two-photon properties are computed using the recently developed polarizable embedding response approach. It is found that the hybrid QM/MM molecular dynamics based approach is the most successful one among other employed computational strategies, viz. reproduction of the metal ion-induced blue shift in the absorption wavelength and decrease in the two-photon absorption cross section, which actually is in excellent agreement with experimental data. The mechanism for such metal ion-induced changes in the optical properties is put forward using a few-state model. Possible design principles to tune the two-photon absorption properties of probes are also discussed.

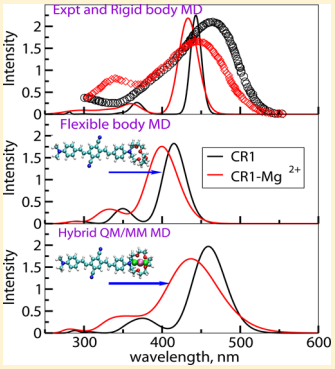

1. INTRODUCTION

Metal ions are essential for life as they play key roles in structure and functioning of many enzymes.[1] It appears that one-third of all enzymes require metal ions for their catalytic activities.[2] Metal ions bind to reactants and align or orient them in favorable ways for the reaction to occur in the catalytic sites which, as a result, reduces the activation energy for the reaction. On the other hand, the rate of enzymatic catalysis is reduced drastically in the absence of metal ions.[3] Besides their pivotal role in the enzymatic catalysis, they serve as structure providers and mediators of interaction between different biological molecules. They also play an important role in maintaining the intracompartmental pH.[4] As examples of importance of metal ions for life activities, eukaryotes and prokaryotes have developed sophisticated mechanisms to extract them from extracellular environments, including mechanisms to transport them to different parts of the cells where they are activated.[5] Transport, storage, and secretion of the metal ions are handled by different cell machineries such as transporters, ion chapperons, and metal-ion storage proteins, to name a few.[5] The human body requires some metal ions in excess, while others are required only in moderate quantity. For example, calcium, iron, sodium, potassium, and zinc are all metal ions needed for the body in large amounts.[1,2,6] At the same time, an excessive body of metal ions and exposure to unwanted metal ions might lead to dysfunction of enzymes and organs and cellular damage. Many neurodegenerative diseases like Wilsons, Parkinson, and Alzheimer's diseases are often associated with an increased level of metal ion concentrations (such as Cu^{2+}, Mn^{2+}, Cd^{2+}, and many others).[7,8] The functioning of different body organelles is thus delicately controlled by maintaining specific concentrations of different metal ions. Following the metal ion distribution, dynamics and transport in cells and body fluids can reveal the normal functioning or malfunctioning of different organelles, and so a normal or diseased state of the human body can be identified.[8]

It follows from the above that many optical, fluorescent, and two-photon probes have been developed to detect and quantitatively estimate specific metal ions within given samples

Received: October 23, 2013
Published: January 8, 2014

or in the human body.[9−11] The chelation of these probes with metal ions is reflected in changes in absorption maximum, fluorescence intensity, or two-photon absorption activity.[9−11] Such chelation might lead to structural or conformational changes (like planarization of the probe), that are the plausible mechanisms of the metal-ion induced changes in the optical property.[12] Among biomedical imaging techniques, two-photon excitation microscopy has gradually gained popularity due to a number of factors,[13,14] such as increased spatial and temporal resolution, the possibility to use near IR or IR radiation for exciting the probes, and the spectral information concerning the microenvironment or the presence of a specific metal ion or biostructure.[15−17] It is important to recognize the causes responsible for the metal-ion induced property change in a given metal ion probe. A major such contribution might in fact come from the structural changes within the probe driven by the metal ions. There are two mechanisms attributed to the metal-ion induced changes in the optical properties, namely "turn-off" and "turn-on", which, respectively, correspond to decrease or enhancement in fluorescence intensity or two-photon absorption cross section.

We aim at understanding various aspects of the metal-ion induced structural and property changes in a mono aza-15-crown-5-ether substituted distyrylbenzene based probe (hereafter referred to as CR1)[18] which falls into the "turn-off" category. The probe in question is known to display a small blue-shift in its absorption spectra and an almost 6-fold decrease in the two-photon absorption cross section when it is bound to a magnesium ion.[18] Static calculations performed by other authors using a semiempirical approach proved to be unsuccessful in explaining the Mg^{2+}-induced changes in the optical property of CR1,[18] and this motivated us to undertake the present study using a more advanced, recently developed, hybrid quantum mechanics/molecular mechanics approach[19,20] for computing optical properties that account for the explicit description of the environment. Several authors[21,22] have emphasized the general importance of sampling over the probe conformation, environment, and finite temperature effects to make a reliable comparison and to gain insight although it is computationally very demanding. We contribute to this effort with an extensive integrated approach-based modeling of the metal-ion probe, CR1, aiming at understanding the molecular mechanism responsible for the blue-shift reported in the probe due to metal-ion binding and decrease in the two-photon absorption cross section. We assess two different computational strategies and select the most suitable one for modeling the metal-ion probe. The first integrated approach combines molecular dynamics for structure modeling and hybrid quantum mechanics/molecular mechanics (QM/MM)[23,24] for the property modeling. In the second integrated approach, we employ the Car−Parrinello hybrid QM/MM molecular dynamics for structure modeling, and again a hybrid QM/MM response approach to determine the optical properties. In particular, a polarizable embedding scheme is used in the latter type of calculations.[19,20] These computational strategies are applied to study the one- and two-photon absorption properties of the probe in acetonitrile (ACN) solvent and when it is bound to the magnesium ion. In order to quantify the effect of the ion, we also study the probe alone in an ACN solvent and compare the computed values against the available experimental results.[18]

2. COMPUTATIONAL DETAILS

We have studied the mono azacrown ether substituted donor−acceptor−donor distyrylbenzene (CR1) in free form, in ACN solvent and when it is bound to a Mg^{2+} ion. As studied in the original experimental paper, the central phenyl group has two cyano groups connected at the para position. Both static and dynamic approaches were employed in order to understand the importance of sampling in modeling the optical properties of this metal ion probe. In what follows, we briefly outline these two computational approaches.

2.1. Static Calculations. The molecular geometry of CR1 in its free state and in its Mg^{2+} bound state is optimized in the ACN solvent described using the polarizable continuum model.[25] In particular, the crown ether is the site where the metal ions bind, and for the optimization of the Mg^{2+} bound probe we use such an initial configuration where the ion is in coordination with nitrogen and oxygen sites of the azacrown ether. Moreover, the Mg^{2+} bound CR1 also includes two chloride ions for making the whole system neutral. Density functional theory with the B3LYP functional and 6-311+G** basis set has been adopted for this optimization using the Gaussian 09 software.[26] We shall refer to the metal-free and metal-bound probe as CR1 and Mg@CR1, respectively. During the optimization procedure, the cavity of the probe was built using the UAHF parameter set. The optimized molecular geometries of CR1 and Mg@CR1 are shown in Figures 1a and

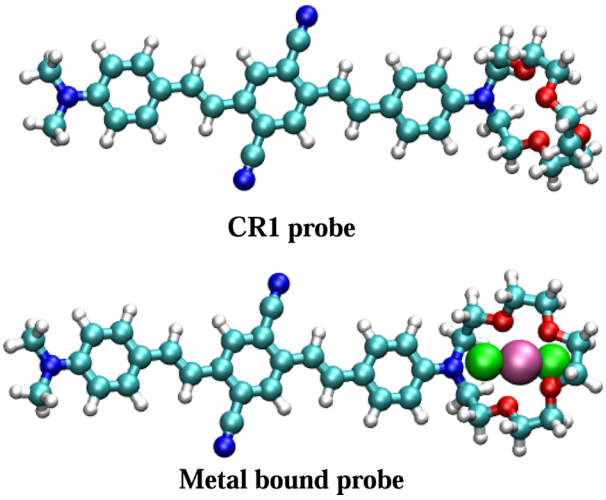

Figure 1. Molecular structure of azacrown ether substituted distyrl benzene probe in its free and Mg^{2+} ion bound state.

1b, respectively. It is worthwhile noting that the geometry of the aza-crown ether moiety is not the same in the case of CR1 and Mg@CR1 which reflects that Mg^{2+} alters the geometry of the crown-ether. As discussed in the next section, however, the geometry changes along the conjugation pathway are minor. The one- and two-photon properties were calculated for these optimized geometries using linear and quadratic response functions as implemented in the DALTON 2.0 program.[27] Details for these calculations are provided below. The solvent effects are taken into account using the polarizable continuum model.[25]

2.2. Rigid and Flexible Probe Molecular Dynamics Simulations. The optimized molecular geometries of CR1 and Mg@CR1 were used as the initial geometries for the subsequent molecular dynamics simulations. The atomic

dx.doi.org/10.1021/ct400924u | J. Chem. Theory Comput. 2014, 10, 778−788

charges obtained by fitting to the molecular electrostatic potential using the CHELPG procedure,[28] as implemented in the Gaussian 09 program, were used to describe the electrostatic interaction of these two systems. The CR1-acetonitrile system includes a single CR1 molecule solvated by 4061 ACN molecules. In the case of Mg@CR1, we considered one CR1 molecule, one Mg^{2+} ion, 4579 ACN molecules, and two chloride ions. For all the solute−solvent subsystems, we employed the General Amber Force Field (GAFF).[29] For both systems, the simulations were carried out in an orthorhombic box. For the former system the initial cell lengths used are approximately 95, 76, and 78.6 Å, and for the latter one the values correspond to 101, 76, and 83 Å. The simulations were carried out within the isothermal−isobaric ensemble at room temperature and 1 atmospheric pressure which assures that the density for both systems evolves to appropriate value. The time step for the integration of equation of motion was kept to be 1 fs, and the total time scale of the simulations was around 20 ns. A cutoff of 10 Å was employed for computing the van der Waals and electrostatic interactions. For all the simulations, we have used AMBER 11 software.[30] The equilibration run for both systems was carried out until the density and total interaction energy reached a convergence threshold. After equilibration, the trajectories were stored for further analysis of the structure and for computing one- and two-photon properties. The molecular geometries of the free probe and metal bound probe are controlled by the employed force-field and which, in turn, dictates the optical properties of these molecules. It is important to estimate the contributions coming from the molecular vibrations and conformational flexibility as predicted by the GAFF force-field. For this purpose, we carried out a new set of simulations where CR1 and Mg@CR1 are treated as rigid bodies, while the remaining subsystem is treated using flexible molecular models. Throughout, the flexible and rigid body simulations for Mg@CR1, the chloride ions were coordinated to the Mg^{2+} ion. The bond length distributions of Mg−Cl from the flexible body MD are shown in the Figure 1S of the Supporting Information.

2.3. Car−Parrinello Hybrid QM/MM Molecular Dynamics Simulations. The final equilibrated configuration from the flexible body molecular dynamics runs for CR1 and Mg@CR1 were used as the input configuration for the Car−Parrinello molecular dynamics within the quantum mechanics-molecular mechanics (QM/MM) framework. We have described CR1 as the QM region, while the solvents were included in the MM region when simulating CR1 in acetonitrile solvent. However, in the case of Mg@CR1, CR1 constitutes the QM part, while the solvent, Mg^{2+}, and the two Cl^- ions were included in the MM region. In both systems studied the net charge of the QM system remains zero. It would have been advantageous to include the Mg^{2+} or the $Mg(Cl)_2$ group in the QM region which would have accounted for the mutual polarization and charge transfer between CR1 by the metal ion. However, due to the availability of the suitable magnesium pseudopotential, we have adopted the procedure as described above. Nevertheless, these effects have been shown to be mostly important for property calculations[31] and not so important for structure modeling itself. In fact as we will see below, the hybrid QM/MM response approach accounts for such effects in the calculation of one- and two-photon properties, and this makes this current work an important contribution to the subject of metal probes modeling using advanced computational approaches. The QM and MM subsystems are modeled by the CPMD[32] and the GROMOS[33] packages, respectively, while the interactions between the QM and MM subsystems are handled by interface code[34] that communicates between the CPMD and GROMOS softwares. The QM/MM Hamiltonian accounts for van der Waals and electrostatic interactions between the QM and MM subsystems. In other words, the polarization of the QM subsystem by the MM system is incorporated additionally during the simulation which is missing in the force-field molecular dynamics simulations. In these hybrid QM/MM molecular dynamics simulations, the QM system is described using the BLYP[35,36] exchange-correlation functional. The wave function for the QM system is expanded in a plane wave basis set, and the number of plane waves were decided by an energy cutoff of 80 Ryd. The interactions between the nucleus and core−electrons are accounted by the pseudopotential located on the atomic centers. The time evolution of the whole system is dictated by the Car−Parrinello Lagrangian within a QM/MM framework.[23,24] The time step for the integration of equations of motion was chosen to be 5 au (0.1 fs). The simulation starts with a quenching run which brings the system to the local minimum on the Born−Oppenheimer potential energy hypersurface. Further scaling and Nose runs are carried out to bring the system temperature to the room temperature. The canonical ensemble is assumed in the simulations. The total time scale of the simulation was around 30 ps for both systems. The instantaneous structures were stored for further analysis and for the purpose of computing the one- and two-photon absorption properties of the CR1 and Mg@CR1 systems (the details concerning the property calculations using TD-DFT within a QM/MM framework are described in the following section). As can be seen from Mg−Cl distributions in Figure 1S of the Supporting Information the chloride ions are bound to the magnesium throughout the simulation. We note that CPMD predicts the bond lengths to be slightly shortened when compared to the MD values. It is worthwhile mentioning that the chloride ion positions are not constrained in the simulation and that they are free to move within the solution. However, they prefer to be in the metal ion bound state which has to be attributed to the favorable electrostatic interaction with the metal ion.

2.4. Hybrid QM/MM Response. The one- and two-photon absorption spectra were computed using linear and quadratic response functions within a TD-DFT/MM framework. The probe subsystem is described using density functional theory, while the remaining subsystems are described using a molecular mechanics force-field. In particular, we employ the polarizable embedding (PE) approach[19,20] to account for the interactions between the QM and MM subsystems. In the case of the CR1-ACN system, the probe is treated using density functional theory, while in the case of Mg@CR1 in ACN, CR1, Mg^{2+}, and the two chloride ions were treated using DFT. This was feasible, since in all simulations, the chloride ions are bound to the Mg^{2+} ion (we refer to the Mg−Cl distance distribution shown in Figure 1S of the Supporting Information). By this we account for the polarization, charge transfer, and electrostatic interaction between the probe and the metal. Particularly, as we will see, facilitating the charge transfer is important to correctly model the metal ion induced changes in the optical property of the probe. As in the case of "static" calculations the CAM-B3LYP exchange-correlation functional[37,38] has been used for one- and two-photon property calculations since it is highly suitable for the description of charge-transfer excited states

which often determines the spectral features in the case of molecular probes.[39] In fact, our recent results of calculations of two-photon absorption spectra of large organic systems proved that the performance of the CAM-B3LYP functional is satisfactory.[40,41] We employ the TZVP[42] basis set which has been tested many times[43−46] and identified to be suitable for optical property calculations of molecular probes. The description of ACN in the TD-DFT/MM calculations was based on atomic point charges and atomic isotropic polarizabilities. The atomic charges were derived following a similar strategy as defined above for the molecules in the classical MD but now using the aug-cc-pVDZ basis set. The atomic polarizabilities were calculated at the level of B3LYP/aug-cc-pVDZ using the LoProp[47] approach as implemented in the MOLCAS[48] software. The polarizable embedding calculations were carried out for the configurations obtained from the molecular dynamics (both for the case of rigid and flexible probes) and hybrid QM/MM molecular dynamics. The number of configurations used for calculating the averaged one- and two-photon absorption spectra is 50. Along with this, the property calculations were carried out for the optimized geometries of CR1 and Mg@CR1 with solvent effects accounted for through the polarizable continuum description.[25]

3. RESULTS AND DISCUSSIONS

3.1. Metal Ion-Induced Structural Modifications in the Probe. First, in this section, we discuss the structure of the azacrown ether substituted distyryl benzene alone in acetonitrile and when it is in chelation with the Mg^{2+} ion. The analysis has been carried out for all three structural cases, namely (i) static structure, (ii) dynamic structures from force-field MD, and (iii) dynamic structure from Car−Parrinello MD. In particular, we are interested in studying whether the chelation brings in any structural changes in the conjugation pathway, which, in turn, might contribute to the metal-chelation induced changes in the optical properties of the metal probe. The conformation of the azacrown ether might be strongly controlled by the metal-ion chelation - it is not clear, however, whether this might also contribute to the changes in the optical property. There exist many detailed reports on how the structure along conjugation pathway controls linear and nonlinear optical properties,[49,50] and for this reason, the structure of the probe along the conjugation pathway and with respect to the conformation of the azacrown ether has been studied. The conjugation pathway was analyzed by computing the average bond lengths, where both the free and metal-bound probe showed alternating single and double bonds between the central and terminal phenyl groups. The average value of the bond lengths are given in Table S1 in the Supporting Information for all three cases. Based on the MD study, we did not observe any significant change in the bond lengths of CR1 due to the metal chelation. However, the static and CPMD simulation results suggest that the NC bond of the phenyl azacrown ether group increases significantly due to the metal chelation (we refer to the values corresponding to CR1 and Mg@CR1 in the Table S1). It is also worthwhile to note that the average bond lengths as obtained from MD and CPMD for CR1 and Mg@CR1 are slightly different which might be reflected in their optical properties.

The conformation of azacrown ether has been analyzed by computing two sets of distance distribution functions: (i) the distance distribution of N, O atoms of azacrown ether with the center of mass of azacrown ether and (ii) the distance distribution of the N atom with the remaining four oxygen atoms of the azacrown ether group. The results, based on the molecular dynamics trajectory, are presented in Figures 2 and 3

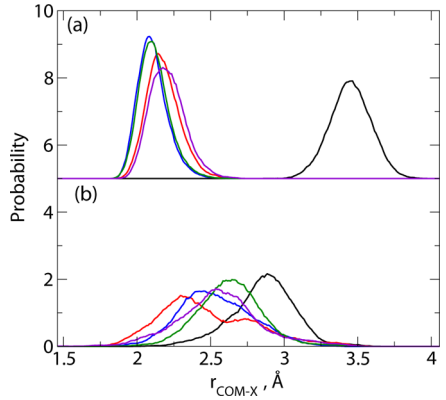

Figure 2. The distribution of R_{com-X} obtained using molecular dynamics trajectory. Here, R_{com-X} refers to the distance between the center-of-mass of the azacrown ether group and nitrogen (shown in blue color in Figure 1) and oxygen atoms (shown in red color) of the same group. There are five different distribution curves corresponding to single N and four O atoms. The figure in the bottom panel corresponds to the free probe, and the one in the top panel corresponds to the metal-bound case. In both cases, the black color corresponds to R_{com-N}, while the remaining four curves correspond to R_{com-O}.

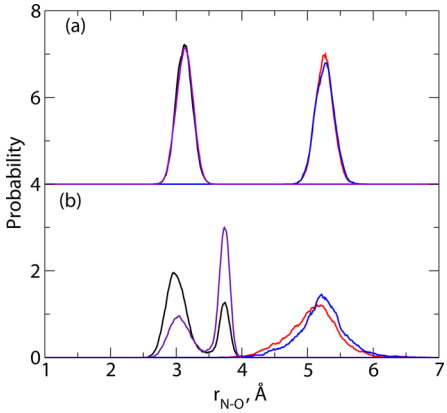

Figure 3. The distribution of R_{N-O} lengths calculated from MD trajectory. Here, R_{N-O} corresponds to the distance between nitrogen and oxygen atoms of azacrown ether group. There are four different distribution curves each corresponding to one oxygen atom of azacrown ether group. The figure in the bottom panel corresponds to the free probe, and the one in the top panel corresponds to metal-bound case.

(the results of calculations using the hybrid QM/MM molecular dynamics will be discussed below). However, considering the long time scale associated with the conformational dynamics, one should expect a better convergence pattern from molecular dynamics. In particular, the inset *a* refers to the case where the metal is bound to the probe, while the results corresponding to free probe are presented in the inset *b*. As it can be clearly seen, the azacrown ether group of the probe in its metal chelated state has more ordered structure than when it is free. The four oxygen atoms are located at similar distances from the center of mass in this case. Similar pattern is found for the corresponding N−O distances as

dx.doi.org/10.1021/ct400924u | J. Chem. Theory Comput. 2014, 10, 778−788

shown in Figures 3a and 3b. With respect to distances, the four oxygen atoms are grouped into two sets. Two oxygen atoms in each set are equidistant from the nitrogen. The two sets of oxygen atoms are maintained in the case of the metal-ion free probe. However, the distance distribution curve is wider suggesting an increased disorder in the conformation of the azacrown ether. Figures 4 and 5 refer to the same length

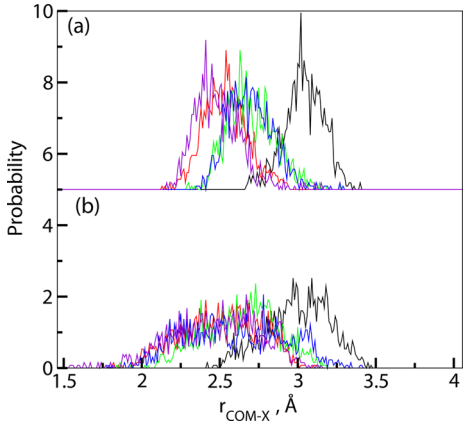

Figure 4. The distribution of R_{com-X} obtained using the hybrid QM/MM molecular dynamics trajectory. The figure in the bottom panel corresponds to the free probe, and the one in the top panel corresponds to the metal-bound probe.

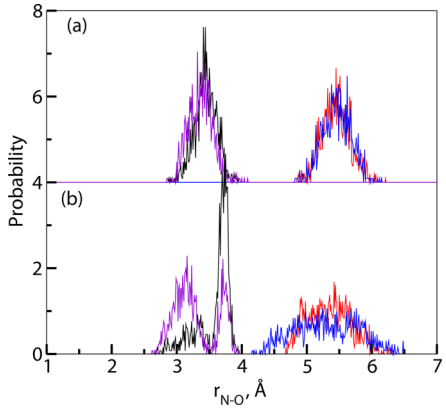

Figure 5. The distribution of R_{N-O} lengths obtained from hybrid QM/MM MD trajectory. The figure in the bottom panel corresponds to the free probe, and the one in the top panel corresponds to the metal-bound probe.

distributions, but now the results correspond to the CPMD trajectory. A very similar behavior is found as in the case of the MD results: The free probe is conformationally disordered, while the metal-bound probe possesses a highly ordered structure. We also note that the average conformational geometry of the metal bound probe obtained from force-field MD is comparable to the hybrid QM/MM molecular dynamics. This suggests that the employed force-field is reasonable in reproducing the conformational geometry of the azacrown ether. Overall, we can see that the metal chelation brings some order into the azacrown ether even though it does not incorporate any significant structural changes within the conjugation pathway of the azacrown ether substituted distyrylbenzene probe. With this background on the metal-chelation induced structural changes in the probe, we will move on to a discussion about its one- and two-photon absorption properties.

3.2. Metal Ion-Induced Modulation of One-Photon Absorption Properties. The average vertical excitation energies corresponding to the four lowest energy transitions are presented in Table 1. As mentioned earlier, this averaging

Table 1. One-Photon Absorption Based on Static and Dynamic Calculations[a]

One Photon Absorption Spectra			
excitation	crown ether	Mg^{2+}-bound crown ether	shift
Experiment[18]			
1	468	445	−23
Static: QM/PCM+QM/PCM			
1	445(2.32)	440(2.27)	−5
2	368(0.27)	364(0.25)	
3	350(0.01)	340(0.08)	
4	300(0.00)	295(0.00)	
Dynamic: Rigid MD+QM/MM Response			
1	442(2.26)	433(2.19)	−9
2	367(0.27)	361(0.20)	
3	347(0.03)	338(0.08)	
4	300(0.01)	307(0.02)	
Dynamic: Flexible MD+QM/MM Response			
1	415(1.83)	400(1.76)	−19
2	353(0.29)	341(0.23)	
3	341(0.12)	323(0.18)	
4	301(0.03)	295(0.04)	
Dynamic: Hybrid QM/MM-MD+ QM/MM Response			
1	459(1.97)	437(1.68)	−22
2	377(0.32)	362(0.32)	
3	355(0.11)	332(0.22)	
4	307(0.03)	296(0.03)	

[a]The results for the absorption wave lengths are in nm. Numbers in parentheses refer to the oscillator strength.

has been carried out for sets of 50 configurations extracted from the molecular dynamics and hybrid QM/MM molecular dynamics simulations. In particular, we have two sets of results for MD corresponding to rigid and flexible body MD. Also results from the static calculations (where the solvent effect is incorporated through the polarizable continuum model) and from experiment[18] are presented. The experimental absorption band maximum (λ_{max}) for the first band is given for the free CR1 and in the presence of Mg^{2+} ions.[18] These experimental results show a blue shift by 23 nm due to metal chelation of the CR1 probe (λ_{max} for the free probe is 468 nm while when bound to the metal ion it is 445 nm). In order to support the choice of the CAM-B3LYP functional for the present study, we have estimated the excitation wavelength corresponding to the transition to the first excited state using the B3LYP functional. The latter value is equal to 626 nm and is largely overestimated in comparison with experimental result. Below, we compare the performance of static and dynamic approaches in predicting the experimental absorption spectra and the metallochromic shift in the CR1 probe. However, it is important to notice that in the case of the static approach and the dynamic approach corresponding to rigid-body simulations of the probe and the metal-bound probe, we present the vertical excitation energies calculated at the equilibrium geometries of the solute. The other two dynamic approaches in fact account for ground state nuclear motions and so often have been directly compared to

the experimental absorption maximum.[51] However, it should be highlighted that none of the approaches applied here accounts for differences in zero-point energies of the ground and excited states of these systems.[52,53] The value of metal chelation-induced shift in the probe as obtained from static approach is underestimated; however, the sign of the metallochromic shift is correctly reproduced. Among the four excitations, the lowest one is the one associated with the largest oscillator strength. This is true in the case of all employed computational strategies, viz. static calculations, dynamic sampling of MD or CPMD.

Looking at the one-photon absorption results obtained as a dynamical average corresponding to the snapshots from MD (both rigid and flexible approaches) one finds that the excitation energies and the metal chelation-induced shift computed from rigid body simulations are comparable to those from the static calculations. This suggests that contributions coming from the configurational sampling of the environment does not have a substantial effect on these properties. However, the flexible body MD results differ significantly compared to the static and rigid-body MD simulations. Here, the sign and the magnitude of the metal chelation induced shift are better reproduced than from the static calculations. However, the average vertical excitation energies of the low energy band values are underestimated to a large extent (i.e., approximately by 45 nm) when compared to the experimental λ_{max}. The finite temperature molecular geometry of both CR1 and Mg@CR1 in flexible body MD is dictated by the employed force-field, and so its inability to describe the ground state geometry in ACN solvent has to be attributed to the failure by this set of calculations in reproducing the one-photon absorption spectra. We note here that for this reason the rigid body simulations are often employed in integrated approaches for the modeling of optical and NMR spectra.[54,55]

We recollect that the MD predicted geometry along the conjugation pathway is slightly different from that based on CPMD. However, since we use an optimized geometry the results from the rigid-body simulation are comparable to the results obtained using the static approach. The OPA results obtained from dynamical averaging of CPMD snapshots appear to be more favorable as the metal chelation-induced shift and the absolute λ_{max} of CR1 and Mg@CR1 agree better with experiments. The computed full absorption spectra, comprising the four lowest energy excitations from dynamical averaging, is shown in Figure 6. As described earlier,[56] the full width at half-maximum for fitting each band has been obtained from the standard deviation associated with each specific excitation. It is interesting to note that the employed approaches could correctly reproduce the decrease in the intensity of the first band of the probe due to the metal chelation as in experiments.[18] The frontier orbitals involved in the intense low-energy excitation and orbital diagrams are presented in Figure 7a and 7b. The excitation appears to have intramolecular charge-transfer character from the two donor groups, namely dimethyl amino and nitrogen of azacrown ether, to the central electron deficient dicyanosubstituted phenyl group. The chelation with the positively charged magnesium ion stabilizes the ground state of the probe, and this, in turn, might be responsible for the obtained blue shift in the absorption spectra.

3.3. Metal Ion-Induced Modulation in the Two-Photon Absorption Properties. We analyze the two-photon absorption spectrum of the probe in its free state and when it is

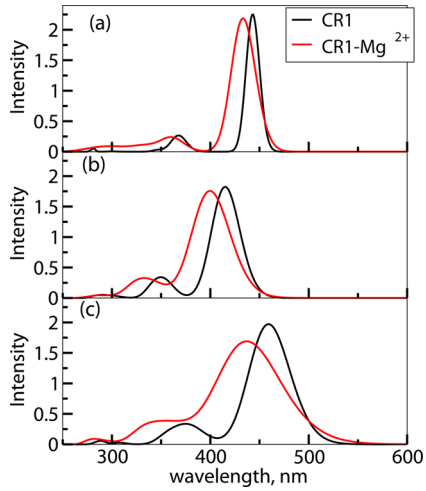

Figure 6. The computed absorption spectra for CR1 and Mg@CR1 as obtained from various sampling procedures. (a) Rigid body simulations (only CR1 and Mg@CR1 are treated as rigid bodies with the geometry obtained from the B3LYP/6-311+G(d,p) level of theory). (b) Flexible body molecular dynamics simulations. (c) Car–Parrinello hybrid QM/MM molecular dynamics simulations.

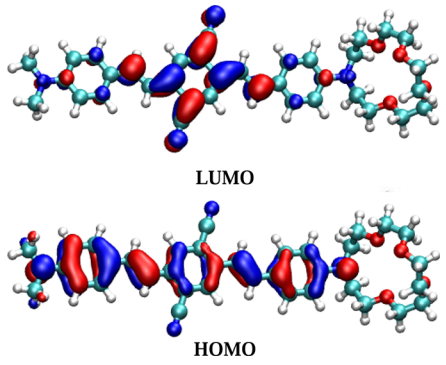

Figure 7. HOMO and LUMO molecular orbitals of the free probe.

bound to Mg^{2+}. As in the case of OPA calculations for the metal bound probe, the neutral molecular state (with 2 chloride ions included) is considered. The two-photon absorption cross section, $\sigma^{2PA}(2\omega)$, in Göppert-Mayer units was computed using the following expression

$$\sigma^{2PA}(2\omega) = \frac{4\pi^3 \alpha a_0^5 \omega^2}{c} g(2\omega)\delta^{2PA} \quad (1)$$

where α is the fine structure constant, a_0 is the Bohr radius, c is the speed of light, ω is the energy of the photon, $g(2\omega)$ is the line shape function, and δ^{2PA} is the two-photon cross section in atomic units.

For the line shape function, we have assumed a Gaussian function of the following form

$$g(2\omega) = \frac{1}{\sigma\sqrt{(2\pi)}} \exp\left(\frac{-(2\omega - \omega_f)^2}{2\sigma^2}\right) \quad (2)$$

where σ is the standard deviation corresponding to the Gaussian distribution of the vertical excitation energy. In theoretical reports using the static approach there is no way to estimate Γ (equal to $2\sigma(2\ln 2)^{1/2}$) and based on the experience from experimental OPA results it is mostly empirically chosen as 0.1 eV.[57−59] There are other reports using a value for Γ in

dx.doi.org/10.1021/ct400924u | J. Chem. Theory Comput. 2014, 10, 778−788

the range 0.05−0.5 eV.[60,61] The nontransferability of the value of Γ between different chemical systems has been discussed in the literature explaining the importance of estimating this value in a nonempirical way.[58] We have shown in previous two papers how to estimate the width of the line shape function for the one photon absorption spectra from integrated approach based calculations that account for dynamics and sampling over solute−solvent configurations.[45,62] In this work, we use the same Gaussian-like line shape function (refer to eq 2) for the TPA calculation to be consistent with the one used in one-photon absorption spectra calculation. We have computed the TPA cross section values using this "dynamic" Γ computed from simulation as well as using the commonly assumed value Γ = 0.1 eV.[57−59] The TPA values obtained from the static approach and three dynamical averaging procedures are presented in Table 2 along with the experimental results.[18]

Table 2. Two Photon Absorption Based on Static and Dynamic Calculations and the Results Are in Units of GM[a]

Two Photon Absorption Spectra		
excitation	crown ether	Mg^{2+}-bound crown ether
Experiment[18]		
1	1800	300
Static Calculations		
1	(11)	(14)
2	(0)	(0)
3	(6069)	(5792)
4	(3479)	(4219)
Dynamic: Rigid MD+QM/MM Response		
1	143(138)	169(349)
2	5(9)	3(8)
3	5603(7582)	1143(4514)
4	2609(4288)	619(4829)
Dynamic: Flexible MD+QM/MM Response		
1	101(248)	115(405)
2	304(715)	101(376)
3	1948(3933)	787(2595)
4	413(1081)	364(1147)
Dynamic: QM/MM-MD+QM/MM Response		
1	78(225)	77(378)
2	168(532)	131(614)
3	2718(6489)	971(3732)
4	2490(5274)	1619(4958)

[a]The results corresponding to the fixed Γ = 0.1 eV are given in parentheses.

Only one set of TPA values is shown for the static case, since these values correspond to a single optimized snapshot. It is found experimentally that there is a 6-fold decrease in the two-photon absorption cross sections due to chelation with Mg^{2+} ion (cf. Table 2). As can be seen from the static calculations, unlike in the case of the two lowest excitations, two-photon transitions to the third and fourth excited states are characterized by significant values of the two-photon absorption cross section. However, the approach relying on the dynamical averaging yields nonzero two-photon absorption intensity even for the first two excitations which has to be attributed to finite temperature and environmental effects. In any case, in agreement with the results from the static calculations, the third and fourth excitations are associated with intense two-photon absorption processes. It is interesting to notice that the first excitation is intense with respect to the one-photon absorption process, while it is not intense with respect to two-photon absorption process. It is important to remember that the symmetry rules governing the allowed transitions are different for these two absorption processes.[63−65] We attribute the third intense two-photon absorption process to the experimentally reported two-photon absorption band as there is a correspondence of the absorption wavelength and intensity. It can clearly be seen that the decrease in the two-photon absorption cross section in the metal bound state of the probe is only marginal for the case of static calculations. Moreover, the absolute values of TPA for free probe and metal-bound probe are larger than the experimental values by ≈3 and 20 times, respectively. Interestingly, all the results from dynamical averaging show a substantial decrease in the TPA intensity as reported from experiments.[18] So, the neglect of the sampling effect appears to be responsible for the failure of the earlier theoretical attempt in predicting the metal ion induced changes in the TPA properties of CR1.[18] We note that the TPA values from sampling based on a commonly used Γ reproduce the overall trend, while the actual magnitudes are manifold larger which clearly demonstrates the need for estimating its value from simulations. For this reason, the following discussion is restricted to the TPA values obtained using the "dynamic" Γ values specific to the system and the excitation.

Interestingly, the rigid body MD predicts almost a 5-fold decrease in the TPA values for the metal-bound probe and outperforms the flexible body MD in this aspect. This clearly indicates the importance of having a correct geometry for the probe in its free and metal-bound case to accurately compute the TPA properties. When compared to the average TPA results obtained from hybrid QM/MM MD, the rigid-body MD results are overestimated for both the free probe and the metal bound probe. Overall, the TPA results corresponding to hybrid QM/MM MD based structure are better among the three dynamical approaches employed. We emphasize that the averaging scheme also predicts that the fourth excitation corresponds to an intense two-photon absorption cross section. However, the wavelength of the photons corresponds nearly to the IR region. The first intense two-photon transition corresponds to the excitation from the ground to the third excited state. In the one-photon picture, this transition involves the HOMO-1 and LUMO one-electron excitation. These orbitals are shown in Figure 8. As seen, there is a density reorganization from the phenyl groups to the central dicyanophenyl group showing an intramolecular charge transfer character. The corresponding molecular orbitals (HOMO-1,

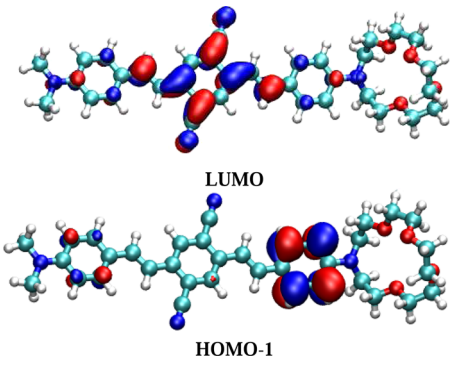

Figure 8. HOMO-1 and LUMO molecular orbitals of the free probe which are involved in the intense two-photon excitation.

dx.doi.org/10.1021/ct400924u | J. Chem. Theory Comput. 2014, 10, 778−788

HOMO, and LUMO) for the metal bound probe are shown in Figure 2S of the Supporting Information.

It is common that an excitation with charge transfer character has intense two-photon absorption cross sections.[17,66] Among the design principles proposed to enhance the two-photon absorption cross section, the most relevant one for this discussion is to increase the intramolecular charge transfer character. Presumably, adding electron donating groups to the phenyl group will increase the two-photon absorption cross section of the probe, while the electron withdrawing groups might bring the reverse effect. In fact, precisely the second effect is responsible for the decrease in the TPA when the probe binds to a positively charged metal ion.

3.4. Few State Model Calculations for TPA. In order to gain insight into the changes of the two-photon absorption cross section of the crown ether upon chelation, a few-state model[67] has been employed. This model, which is a special case of a generalized few-state model proposed by Alam et al.,[68] considers three electronic states: ground ($|0\rangle$), intermediate ($|1\rangle$), and final ($|3\rangle$). We note that the excited state $|3\rangle$ is also included as an intermediate in our treatment. The two-photon absorption probability corresponding to excitation from the ground to the third excited state is given by

$$\delta_{\mathrm{TLM}}^{3\leftarrow 0} = \delta^{11} + \delta^{33} + 2\delta^{13} \tag{3}$$

where

$$\delta^{11} = \frac{4}{15}\left(\frac{|\mu^{01}||\mu^{13}|}{\omega_1 - \frac{1}{2}\omega_3}\right)^2 (2\cos^2(\theta_{13}^{01}) + 1) \tag{4}$$

$$\delta^{33} = \frac{8}{15}\left(\frac{|\mu^{03}||\mu^{33}|}{\omega_3}\right)^2 (2\cos^2(\theta_{33}^{03}) + 1) \tag{5}$$

$$\delta^{13} = \frac{8}{15}\left(\frac{|\mu^{01}||\mu^{03}||\mu^{13}||\mu^{33}|}{\omega_3\left(\omega_1 - \frac{1}{2}\omega_3\right)}\right)(\cos\theta_{03}^{33}\cos\theta_{01}^{13} + \cos\theta_{03}^{01}\cos\theta_{33}^{13} + \cos\theta_{03}^{13}\cos\theta_{01}^{33}) \tag{6}$$

Here $\hbar\omega_i$ stands for the excitation energy from the ground state to the excited state $|i\rangle$, $\mu^{ij} = \langle i|\vec{\mu}|j\rangle$, and θ_{ij}^{kl} is the angle between (transition) dipole moments μ^{ij} and μ^{kl}. A schematic representation of the various optical channels involving these terms is presented in Figure 9. We have determined $\delta_{\mathrm{TLM}}^{3\leftarrow 0}$ using the polarizable embedding TD-DFT for two uncorrelated configurations of crown ether and one configuration of the chelated crown ether. These configurations have been chosen so that the excitation energies to the third excited state were close to the mean value obtained from the statistical averaging. The results of the calculations of $\delta_{\mathrm{TLM}}^{3\leftarrow 0}$ and its breakdown into various contributions are shown in Table 3. As seen, the δ^{33} term is quite insignificant both for crown ether and for the chelate. The dominant contribution to $\delta_{\mathrm{TLM}}^{3\leftarrow 0}$ for both systems is due to the δ^{11} term and its decrease upon Mg^{2+} chelation follows the pattern observed for two-photon absorption probability reported in the last column of Table 3. In fact, we have inspected the quantities contributing to δ^{11}, and its decrease can be directly related to the increase of excitation energy ω_1 and decrease of $|\mu^{01}|$. The optical channel involving the intermediate state $|1\rangle$ is by far the most important one in two-photon absorption from the ground to the third excited state, viz. δ^{ii} $(i \neq 1)$ corresponding to channels involving other intermediate states $|i\rangle$ are several orders of magnitude smaller (results are not shown). The interference term δ^{13} is negative for all three configurations shown in Table 3 and is rather insignificant in terms of magnitude. Finally, we note that the values of $\delta_{\mathrm{TLM}}^{3\leftarrow 0}$ are in good agreement with the results determined using response theory.

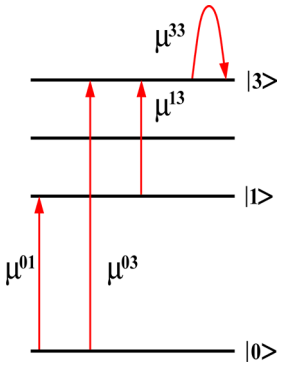

Figure 9. Schematic representation of optical channels considered in the few-state model. $|0\rangle$, $|1\rangle$, and $|3\rangle$ correspond to the ground, intermediate, and the final state, respectively. The latter state is also included in the model as the intermediate state.

Table 3. Breakdown of the Two-Photon Absorption Probability Using the Three-Level Approximation ($\delta_{\mathrm{TLM}}^{3\leftarrow 0}$, cf. Eq 3)[a]

	δ^{11}	δ^{33}	δ^{13}	$\delta_{\mathrm{TLM}}^{3\leftarrow 0}$	$\delta_{\mathrm{exact}}^{3\leftarrow 0}$
crown ether (#1)	434	4	−38	362	452
crown ether (#2)	550	1	−2	547	520
Mg^{2+} crown ether	264	1	−8	249	246

[a] $\delta_{\mathrm{exact}}^{3\leftarrow 0}$ stands for the "exact" value determined with the aid of response theory. All values are given in au and should be multiplied by 10^3.

3.5. Conclusions. In this paper we have undertaken a study on the structure and optical properties of azacrown ether substituted distyryl benzene in its free and metal-ion bound state embedded in acetonitrile solvent. Our study is partly motivated by that a previous attempt to model the optical properties of this system was shown to be unsuccessful and partly due to the availability of sophisticated QM/MM approaches for modeling structure and properties of complex systems which could have an important bearing on problems concerning metal ion probing in bioenvironments. Our work leads to conclusions of general and detailed character. Among the latter we find that the results for the absorption spectra of the probe and metal bound probe based on rigid-body molecular dynamics are better than the flexible body molecular dynamics. The results based on hybrid QM/MM structure and property modeling correctly reproduce the metal-induced shift in the absorption spectra of the probe. Moreover, the one and two-photon spectra of the free probe and metal bound probe are well reproduced in agreement with experimental results. We attribute the negligence of sampling effects to be responsible for the failure of the earlier theoretical attempt in reproducing the metal ion induced changes in the TPA properties of this probe. The decrease in the two-photon absorption cross section of the probe due to metal chelation has been reproduced something that we attribute to the decrease in the intramolecular charge transfer due to the azacrown ether group binding to the positively charged metal ion. The first band of the probe and metal bound probe is intense with respect to the one-photon

dx.doi.org/10.1021/ct400924u | J. Chem. Theory Comput. 2014, 10, 778−788

absorption process, while it is the third band which becomes intense for the two-photon absorption process. A three state model with the first excited state as the intermediate state acquires most of the two-photon excitation probability suggesting that the optical channel involving the first excited state as the intermediate state is the most important one. By chemical substitution with appropriate electron withdrawing and donating groups, one can control the amount of intramolecular charge transfer from the amino and azacrown ether groups to the central dicyano phenyl group which will eventually alter the two-photon absorption cross sections. Such design principles and structure−property relationships for a metal probes can thus be extracted from the in silico methods as shown here. As the main general conclusion we find that an integrated approach by combining the Car−Parrinello based structure modeling and the hybrid QM/MM response method based optical property modeling was proved to be a promising and effective methodology to study metal chelation induced changes in optical properties of molecular probes.

■ ASSOCIATED CONTENT

Supporting Information

The bond length distributions for Mg−Cl bonds of Mg@CR1 from the flexible body MD and hybrid QM/MM MD are shown in Figure S1. Figure S2 shows HOMO-1, HOMO, and LUMO molecular orbitals of Mg@CR1. The average bond lengths (along the conjugation pathway) for CR1 and Mg@CR1 as obtained from static and dynamic approaches are given in Table S1. This material is available free of charge via the Internet at http://pubs.acs.org.

■ AUTHOR INFORMATION

Corresponding Author

*E-mail: murugan@theochem.kth.se.

Notes

The authors declare no competing financial interest.

■ ACKNOWLEDGMENTS

This work was supported by a grant from the Swedish Infrastructure Committee (SNIC) for the project "Multiphysics Modeling of Molecular Materials", SNIC025/12-38. The work was also financed by a subsidy from the Polish Ministry of Science and Higher Education within "Iuventus Plus" programme (Grant No. 0628/IP3/2011/71). R.Z. is a Wenner-Gren Foundations scholar. J.K. thanks the Danish Center for Scientific Computing (DCSC), The Danish Councils for Independent Research (The Sapere Aude programme), the Lundbeck Foundation, and the Villum foundation for financial support.

■ REFERENCES

(1) Holm, R. H.; Kennepohl, P.; Solomon, E. I. Structural and Functional Aspects of Metal Sites in Biology. *Chem. Rev.* **1996**, *96*, 2239−2314.

(2) Waldron, K. J.; Rutherford, J. C.; Ford, D.; Robinson, N. J. Metalloproteins and Metal Sensing. *Nature* **1996**, *460*, 823−830.

(3) Andreini, C.; Bertini, I.; Cavallaro, G.; Holliday, G.; Thornton, J. Metal Ions in Biological Catalysis: from Enzyme Databases to General Principles. *J. Biol. Inorg. Chem.* **2008**, *13*, 1205−1218.

(4) Casey, J. R.; Grinstein, S.; Orlowski, J. Sensors and Regulators of Intracellular pH. *Nat. Rev. Mol. Cell Biol.* **2010**, *11*, 13518−13523.

(5) O'Halloran, T. V.; Culotta, V. C. Metallochaperones, an Intracellular Shuttle Service for Metal Ions. *J. Biol. Chem.* **2000**, *275*, 25057−25060.

(6) Finney, L. A.; O'Halloran, T. V. Transition Metal Speciation in the Cell: Insights from the Chemistry of Metal Ion Receptors. *Science* **2003**, *300*, 931−936.

(7) Barnham, K. J.; Bush, A. I. Metals in Alzheimer's and Parkinson's Diseases. *Curr. Opin. Chem. Biol.* **2008**, *12*, 222−228.

(8) Robison, G.; Zakharova, T.; Fu, S.; Jiang, W.; Fulper, R.; Barrea, R.; Marcus, M. A.; Zheng, W.; Pushkar, Y. X-Ray Fluorescence Imaging: A New Tool for Studying Manganese Neurotoxicity. *PLoS One* **2012**, *7*, e48899.

(9) Domaille, D. W.; Que, E. L.; Chang, C. J. Synthetic Fluorescent Sensors for Studying the Cell Biology of Metals. *Nat. Chem. Biol.* **2008**, *4*, 168−175.

(10) Formica, M.; Fusi, V.; Giorgi, L.; Micheloni, M. New Fluorescent Chemosensors for Metal Ions in Solution. *Coord. Chem. Rev.* **2012**, *256*, 170−192.

(11) Kim, H. M.; Cho, B. R. Two-Photon Fluorescent Probes for Metal Ions. *Chem. - Asian J.* **2011**, *6*, 58−69.

(12) Ramirez, J.-Z.; Vargas, R.; Garza, J. The Role of Conformational Changes in the Signal Enhancement of a Selective Chemosensor of Pb2+. *Phys. Chem. Chem. Phys.* **2012**, *14*, 495−501.

(13) Zipfel, W. R.; Williams, R. M.; Webb, W. W. Nonlinear Magic: Multiphoton Microscopy in the Biosciences. *Nat. Biotechnol.* **2003**, *21*, 1369−1377.

(14) Myung Kim, H.; Rae Cho, B. Two-Photon Materials with Large Two-Photon Cross Sections. Structure-Property Relationship. *Chem. Commun.* **2009**, 153−164.

(15) Dodani, S. C.; He, Q.; Chang, C. J. A Turn-On Fluorescent Sensor for Detecting Nickel in Living Cells. *J. Am. Chem. Soc.* **2009**, *131*, 18020−18021.

(16) Zeng, L.; Miller, E. W.; Pralle, A.; Isacoff, E. Y.; Chang, C. J. A Selective Turn-On Fluorescent Sensor for Imaging Copper in Living Cells. *J. Am. Chem. Soc.* **2006**, *128*, 10−11.

(17) Sumalekshmy, S.; Henary, M. M.; Siegel, N.; Lawson, P. V.; Wu; Schmidt, K.; Brédas, J.-L.; Perry, J. W.; Fahrni, C. J. Design of Emission Ratiometric Metal-Ion Sensors with Enhanced Two-Photon Cross Section and Brightness. *J. Am. Chem. Soc.* **2007**, *129*, 11888−11889.

(18) Pond, S. J. K.; Tsutsumi, O.; Rumi, M.; Kwon, O.; Zojer, E.; Brédas, J.-L.; Marder, S. R.; Perry, J. W. Metal-Ion Sensing Fluorophores with Large Two-Photon Absorption Cross Sections: Aza-Crown Ether Substituted Donor-Acceptor-Donor Distyrylbenzenes. *J. Am. Chem. Soc.* **2004**, *126*, 9291−9306.

(19) Olsen, J. M.; Aidas, K.; Kongsted, J. Excited States in Solution through Polarizable Embedding. *J. Chem. Theory Comput.* **2010**, *6*, 3721−3734.

(20) Olsen, J. M. H.; Kongsted, J. Molecular Properties through Polarizable Embedding. *Adv. Quantum Chem.* **2011**, *61*, 107−143.

(21) Barone, V.; Baiardi, A.; Biczysko, M.; Bloino, J.; Cappelli, C.; Lipparini, F. Implementation and Validation of a Multi-Purpose Virtual Spectrometer for Large Systems in Complex Environments. *Phys. Chem. Chem. Phys.* **2012**, *14*, 12404−12422.

(22) Biczysko, M.; Bloino, J.; Brancato, G.; Cacelli, I.; Cappelli, C.; Ferretti, A.; Lami, A.; Monti, S.; Pedone, A.; Prampolini, G.; Puzzarini, C.; Santoro, F.; Trani, F.; Villani, G. Integrated Computational Approaches for Spectroscopic Studies of Molecular Systems in the Gas Phase and in Solution: Pyrimidine As a Test Case. *Theor. Chem. Acc.* **2012**, *131*, 1201.

(23) Warshel, A.; Levitt, M. Theoretical Studies of Enzymic Reactions: Dielectric, Electrostatic and Steric Stabilization of the Carbonium Ion in the Reaction of Lysozyme. *J. Mol. Biol.* **1976**, *103*, 227−249.

(24) Field, M. J.; Bash, P. A.; Karplus, M. A Combined Quantum Mechanical and Molecular Mechanical Potential for Molecular Dynamics Simulations. *J. Comput. Chem.* **1990**, *11*, 700−733.

(25) Tomasi, J.; Mennucci, B.; Cammi, R. Quantum Mechanical Continuum Solvation Models. *Chem. Rev.* **2005**, *105*, 2999−3094.

(26) Frisch, M. J.; Trucks, G. W.; Schlegel, H. B.; Scuseria, G. E.; Robb, M. A.; Cheeseman, J. R.; Scalmani, G.; Barone, V.; Mennucci, B.; Petersson, G.; Nakatsuji, H.; Caricato, M.; Li, X.; Hratchian, H. P.; Izmaylov, A. F.; Bloino, J.; Zheng, G.; Sonnenberg, J. L.; Hada, M.; Ehara, M.; Toyota, K.; Fukuda, R.; Hasegawa, J.; Ishida, M.; Nakajima, T.; Honda, Y.; Kitao, O.; Nakai, H.; Vreven, T.; Montgomery, J. A.; Peralta, J. E.; Ogliaro, F.; Bearpark, M.; Heyd, J. J.; Brothers, E.; Kudin, K. N.; Staroverov, V. N.; Kobayashi, R.; Normand, J.; Raghavachari, K.; Rendell, A.; Burant, J.; Iyengar, S. S.; Tomasi, J.; Cossi, M.; Rega, N.; Millam, J. M.; Klene, M.; Knox, J. E.; Cross, J. B.; Bakken, V.; Adamo, C.; Jaramillo, J.; Gomperts, R.; Stratmann, R. E.; Yazyev, O.; Austin, A. J.; Cammi, R.; Pomelli, C.; Ochterski, J. W.; Martin, R. L.; Morokuma, K.; Zakrzewski, V. G.; Voth, G. A.; Salvador, P.; Dannenberg, J. J.; Dapprich, S.; Parandekar, P. V.; Mayhall, N. J.; Daniels, A. D.; Farkas, O.; Foresman, J. B.; Ortiz, J. V.; Cioslowski, J.; Fo, D. J. *Gaussian 09*, Revision A.02; Gaussian, Inc.: Wallingford, CT, 2009.

(27) DALTON, a molecular electronic structure program, Release Dalton 2011. See http://daltonprogram.org/ (accessed May 20, 2013).

(28) Breneman, C.; Wiberg, K. Determining Atom-Centered Monopoles from Molecular Electrostatic Potentials. The Need for High Sampling Density in Formamide Conformational Analysis. *J. Comput. Chem.* **1990**, *11*, 361−373.

(29) Wang, J.; Wolf, R.; Caldwell, J.; Kollman, P.; Case, D. Development and Testing of a General AMBER force field. *J. Comput. Chem.* **2004**, *34*, 1157−1174.

(30) Case, D. A.; Darden, T. A.; Cheatham, T. E.; Simmerling, C. L.; Wang, J.; Duke, R. E.; Luo, R.; Crowley, M.; Walker, R. C.; Zhang, W.; Merz, K. M.; Wang, B.; Hayik, S.; Roitberg, A.; Seabra, G.; Kolossvai, I.; Wong, K. F.; Paesani, F.; Vanicek, J.; Wu, X.; Brozell, S. R.; Steibrecher, T.; Gohlke, H.; Yang, L.; Tan, C.; Mongan, J.; Hornak, V.; Cui, G.; Mathews, D. H.; Seetin, M. G.; Sagui, C.; Babin, V.; Kollman, P. A. *Amber 11*; University of California: San Francisco, CA, 2010.

(31) Nielsen, C. B.; Christiansen, O.; Mikkelsen, K. V.; Kongsted, J. Density Functional Self-Consistent Quantum Mechanics/Molecular Mechanics Theory for Linear and Nonlinear Molecular Properties: Applications to Solvated Water and Formaldehyde. *J. Chem. Phys.* **2007**, *126*, 154112.

(32) Hutter, J.; Parrinello, M.; Marx, D.; Focher, P.; Tuckerman, M.; Andreoni, W.; Curioni, A.; Fois, E.; Röthlisberger, U.; Giannozzi, P.; Deutsch, T.; Alavi, A.; Sebastiani, D.; Laio, A.; VandeVondele, J.; Seitsonen, A.; Billeter, S. Computer code CPMD, version 3.11; Copyright IBM Corp. and MPI-FKF Stuttgart, 1990−2002.

(33) van Gunsteren, W. F.; Billeter, S. R.; Eising, A. A.; Hünenberger, P. H.; Krüger, P.; Mark, A. E.; Scott, W. R. P.; Tironi, I. *Biomolecular Simulation: The GROMOS96 Manual and User Guide*; Vdf Hochschulverlag AG an der ETH Zürich: Zürich, 1996.

(34) Laio, A.; VandeVondele, J.; Rothlisberger, U. A Hamiltonian Electrostatic Coupling Scheme for Hybrid Car-Parrinello Molecular Dynamics Simulations. *J. Chem. Phys.* **2006**, *116*, 6941.

(35) Becke, A. D. Density-Functional Exchange-Energy Approximation with Correct Asymptotic Behavior. *Phys. Rev. A* **1988**, *38*, 3098−3100.

(36) Lee, C.; Yang, W.; Parr, R. G. Development of the Colle-Salvetti Correlation-Energy Formula into a Functional of the Electron Density. *Phys. Rev. B* **1988**, *37*, 785−789.

(37) Yanai, T.; Tew, D. P.; Handy, N. C. A New Hybrid Exchange-Correlation Functional Using the Coulomb-Attenuating Method (CAM-B3LYP). *Chem. Phys. Lett.* **2004**, *393*, 51−57.

(38) Peach, M. J. G.; Helgaker, T.; Sagek, P.; Keal, T. W.; Lutnæs, O. B.; Tozer, D. J.; Handy, N. C. Assessment of a Coulomb-Attenuated Exchange-Correlation Energy Functional. *Phys. Chem. Chem. Phys.* **2006**, *8*, 558−562.

(39) Reichardt, C. Solvatochromic Dyes as Solvent Polarity Indicators. *Chem. Rev.* **1994**, *94*, 2319−2358.

(40) Wielgus, M.; Zaleśny, R.; Arul Murugan, N.; Kongsted, J.; Ågren, H.; Samoc, M.; Bartkowiak, W. Two-Photon Solvatochromism II: Experimental and Theoretical Study of Solvent Effects on the Two-Photon Absorption Spectrum of Reichardt's Dye. *Chem. Phys. Chem.* **2013**, *14*, 3731−3739.

(41) Olesiak-Banska, J.; Matczyszyn, K.; Zaleśny, R.; Arul Murugan, N.; Kongsted, J.; Ågren, H.; Bartkowiak, W.; Samoc, M. Revealing Spectral Features in Two-Photon Absorption Spectrum of Hoechst 33342: A Combined Experimental and Quantum-Chemical Study. *J. Phys. Chem. B* **2013**, *117*, 12013−12019.

(42) Schafer, A.; Huber, C.; Ahlrichs, R. Fully Optimized Contracted Gaussian Basis Sets of Triple Zeta Valence Quality for Atoms Li to Kr. *J. Chem. Phys.* **1994**, *100*, 5829−5835.

(43) Murugan, N. A.; Olsen, J. M. H.; Kongsted, J.; Rinkevicius, Z.; Aidas, K.; Ågren, H. Amyloid Fibril-Induced Structural and Spectral Modifications in the Thioflavin-T Optical Probe. *J. Phys. Chem. Lett.* **2013**, *4*, 70−77.

(44) Murugan, N. A.; Kongsted, J.; Rinkevicius, Z.; Ågren, H. Color Modeling of Protein Optical Probes. *Phys. Chem. Chem. Phys.* **2012**, *14*, 1107−1112.

(45) Murugan, N. A.; Kongsted, J.; Rinkevicius, Z.; Aidas, K.; Mikkelsen, K. V.; Ågren, H. Hybrid Density Functional Theory/Molecular Mechanics Calculations of Two-Photon Absorption of Dimethylamino Nitro Stilbene in Solution. *Phys. Chem. Chem. Phys.* **2011**, *13*, 12506−12516.

(46) Murugan, N. A.; Kongsted, J.; Ågren, H. pH Induced Modulation of One and Two-Photon Absorption Properties in a Naphthalene Based Molecular Probe. *J. Chem. Theory Comput.* **2013**, *9*, 36603669.

(47) Gagliardi, L.; Lindh, R.; Karlström, G. Local Properties of Quantum Chemical Systems: The LoProp Approach. *J. Chem. Phys.* **2004**, *121*, 4494−4500.

(48) Aquilante, F.; De Vico, L.; Ferré, N.; Ghigo, G.; Malmqvist, P.-A.; Neogrády, P.; Pedersen, T. B.; Pitoňák, M.; Reiher, M.; Roos, B. O.; Serrano-Andrés, L.; Urban, M.; Veryazov, V.; Lindh, R. MOLCAS 7: The Next Generation. *J. Comput. Chem.* **2010**, *31*, 224−247.

(49) Bourhill, G.; Bredas, J.-L.; Cheng, L.-T.; Marder, S. R.; Meyers, F.; Perry, J. W.; Tiemann, B. G. Experimental Demonstration of the Dependence of the First Hyperpolarizability of Donor-Acceptor-Substituted Polyenes on the Ground-State Polarization and Bond Length Alternation. *J. Am. Chem. Soc.* **1994**, *116*, 2619−2620.

(50) Meyers, F.; Marder, S. R.; Pierce, B. M.; Bredas, J. L. Electric Field Modulated Nonlinear Optical Properties of Donor-Acceptor Polyenes: Sum-Over-States Investigation of the Relationship between Molecular Polarizabilities (.alpha., .beta., and .gamma.) and Bond Length Alternation. *J. Am. Chem. Soc.* **1994**, *116*, 10703−10714.

(51) De Mitri, N.; Monti, S.; Prampolini, G.; Barone, V. Absorption and Emission Spectra of a Flexible Dye in Solution: A Computational Time-Dependent Approach. *J. Chem. Theory Comput.* **2013**, *9*, 4507−4516.

(52) Jacquemin, D.; Planchat, A.; Adamo, C.; Mennucci, B. TD-DFT Assessment of Functionals for Optical 00 Transitions in Solvated Dyes. *J. Chem. Theory Comput.* **2012**, *8*, 2359−2372.

(53) Adamo, C.; Jacquemin, D. The Calculations of Excited-State Properties with Time-Dependent Density Functional Theory. *Chem. Soc. Rev.* **2013**, *42*, 845−856.

(54) Olsen, J. M.; Aidas, K.; Mikkelsen, K. V.; Kongsted, J. Solvatochromic Shifts in Uracil: A Combined MD-QM/MM Study. *J. Chem. Theory Comput.* **2010**, *6*, 249−256.

(55) Kongsted, J.; Osted, A.; Mikkelsen, K. V.; Åstrand, P.-O.; Christiansen, O. Solvent Effects on the n→π^* Electronic Transition in Formaldehyde: A Combined Coupled Cluster/Molecular Dynamics Study. *J. Chem. Phys.* **2004**, *121*, 8435.

(56) Murugan, N. A.; Rinkevicius, Z.; Ågren, H. Modeling Solvatochromism of Nile Red in Water. *Int. J. Quantum Chem.* **2011**, *111*, 1521−1530.

(57) Albota, M.; et al. Design of Organic Molecules with Large Two-Photon Absorption Cross Sections. *Science* **1998**, *281*, 1653−1656.

(58) Poulsen, T. D.; Frederiksen, P. K.; Jorgensen, M.; Mikkelsen, K. V.; Ogilby, P. R. Two-Photon Singlet Oxygen Sensitizers: Quantifying, Modeling, and Optimizing the Two-Photon Absorption Cross Section. *J. Phys. Chem. A* **2001**, *105*, 11488−11495.

(59) Nayyar, I. H.; Masunov, A. E.; Tretiak, S. Comparison of TD-DFT Methods for the Calculation of Two-Photon Absorption Spectra of Oligophenylvinylenes. *J. Phys. Chem. C* **2013**, *117*, 18170−18189.
(60) Day, P. N.; Nguyen, K. A.; Pachter, R. TDDFT Study of One- and Two-Photon Absorption Properties: π Donor-p-Acceptor Chromophores. *J. Phys. Chem. B* **2005**, *109*, 1803−1814.
(61) Day, P. N.; Nguyen, K. A.; Pachter, R. Calculation of Two-Photon Absorption Spectra of Donor–Acceptor Compounds in Solution Using Quadratic Response Time-Dependent Density Functional Theory. *J. Chem. Phys.* **2006**, *125*, 094103.
(62) Silva, D. L.; Murugan, N. A.; Kongsted, J.; Rinkevicius, Z.; Canuto, S.; Ågren, H. The Role of Molecular Conformation and Polarizable Embedding for One- and Two-Photon Absorption of Disperse Orange 3 in Solution. *J. Phys. Chem. B* **2012**, *116*, 8169−8181.
(63) Kamada, K.; Iwase, Y.; Sakai, K.; Kondo, K.; Ohta, K. Cationic Two-Photon Absorption Chromophores with Double- and Triple-Bond Cores in Symmetric/Asymmetric Arrangements. *J. Phys. Chem. C* **2009**, *113*, 11469−11474.
(64) Ohta, K.; Yamada, S.; Kamada, K.; Slepkov, A. D.; Hegmann, F. A.; Tykwinski, R. R.; Shirtcliff, L. D.; Haley, M. M.; Saek, P.; Gelmukhanov, F.; Ågren, H. Two-Photon Absorption Properties of Two-Dimensional-Conjugated Chromophores: Combined Experimental and Theoretical Study. *J. Phys. Chem. A* **2011**, *115*, 105−117.
(65) Macoas, E.; Marcelo, G.; Pinto, S.; Caneque, T.; Cuadro, A. M.; Vaquero, J. J.; Martinho, J. M. G. A V-shaped cationic dye for nonlinear optical bioimaging. *Chem. Commun.* **2011**, *47*, 7374−7376.
(66) Wilson, J. N.; Bunz, U. H. F. Switching of Intramolecular Charge Transfer in Cruciforms: Metal Ion Sensing. *J. Am. Chem. Soc.* **2005**, *127*, 4124−4125.
(67) Cronstrand, P.; Luo, Y.; Ågren, H. Effects of Dipole Alignment and Channel Interference on Two-Photon Absorption Cross Sections of Two-Dimensional Charge-Transfer Systems. *J. Chem. Phys.* **2002**, *117*, 11102.
(68) Alam, M. M.; Chattopadhyaya, M.; Chakrabarti, S. Enhancement of Twist Angle Dependent Two-Photon Activity through the Proper Alignment of Ground to Excited State and Excited State Dipole Moment Vectors. *J. Phys. Chem. A* **2012**, *116*, 8067−8073.